IEEE Journal of Microwaves

Received 19 June 2023; revised 18 August 2023; accepted 21 August 2023. Date of publication 25 September 2023; date of current version 9 October 2023.

Digital Object Identifier 10.1109/JMW.2023.3313115

Experimental Characterization of a Helical Antenna Integrated in the Rear of a Vehicle for C-V2X Communications

ADAMANTIA CHLETSOU [1] (Student Member, IEEE), ERIC NEWSOM [2], AND JOHN PAPAPOLYMEROU [1] (Life Member, IEEE)

(Regular Paper)

[1]Department of Electrical Engineering, Michigan State University, East Lansing, MI 48824 USA
[2]Ford Motor Company, Dearborn, MI 48126 USA

CORRESPONDING AUTHOR: Adamantia Chletsou (e-mail: chletsou@msu.edu).

ABSTRACT A helical antenna for Cellular-Vehicle To Everything (C-V2X) communications is manufactured and integrated around the car high mount stop light (CHMSL) area of a Ford SUV vehicle. The antenna performance is measured on a foam pillar, on a ground plane and on the vehicle, inside a near field measurement system. The antenna consists of three helical arms wrapped around a 3D-printed hemisphere with a radius of 4.8 mm. The helical arms are built using commercial wire with a radius of 0.127 mm. It operates in a monopole configuration, has an omni-directional radiation pattern and vertical polarization. The maximum measured realized gain of the antenna when integrated on the vehicle is 2.5 dBi at 5.9 GHz.

INDEX TERMS Additive manufacturing, automotive antennas, C-V2X, helical antennas.

I. INTRODUCTION

The recently assigned frequency bands for automotive applications have resulted in an increase on the number of vehicular antennas. Automotive antennas are protruding from body of the car which makes it not practical for increased number of antennas; as a result researchers are investigating the development of miniaturized antennas that can be hidden inside plastic automotive parts. Cellular vehicle to everything communications (C-V2X) were standardized by 3GPP in Release 14 in 2014 and finalized in 2017. C-V2X replaces the Dedicated Short Range Communications (DSRC) and is based on LTE as the underlying technology, connecting the vehicles to other vehicles, to the infrastructure, to pedestrians and the network.

Most antennas for C-V2X applications, found in literature, suggest antenna designs that can be mounted on the rooftop of the vehicle. The rooftop of the vehicle acts as an infinite ground plane, boosting the antenna performance. In [1] Jouini et al. compared the performance of different patch antennas that can be mounted on the rooftop for C-V2X applications, through simulations. Through this study they identified that the inverted L patch antenna (PILA) has the wider beam-width and a gain of 4 dBi. Zhou et al., in [2] simulated a low profile antenna, with a height of 4 mm, vertical polarization, omnidirectional radiation pattern and a maximum simulated gain of 4.5 dBi. In [3] Alavis et al., studied the near field and far field data of antenna measurements for C-V2X communications by using a monocone antenna on the rooftop of a vehicle, through simulations. In [4], Shen et al. suggest a flush mount compact vehicle antenna system that supports 4-channel MIMO operation of LTE, 5 G sub6, WLAN, and C-V2X communications. The antenna has a diameter of 15.2 cm and a height of 2 cm and is mounted on the rooftop of a vehicle during the simulations.

In this research we suggest a helical antenna that can fit inside the rear stop light of a vehicle and meet the requirements of C-V2X communications, identified by Ford. Compared to the literature, we propose a new mounting position for automotive C-V2X communications that to best of our knowledge has not been researched before. The absence of a rooftop, did not affect the suggested antenna performance. The measured antenna radiation properties at the rear of the vehicle meets the requirements for C-V2X applications. This type of antenna compared to PIFA antennas and top-loaded monopoles does not require a rooftop of the vehicle to act as an infinite ground

plane, thus can be used on convertible vehicles or vehicles with plastic rooftops.

II. DESIGN

The antenna design is inspired by Best in [5]. It consists of three spherical helical arms, mounted over a ground plane. As explained in [5] the antenna has a vertical polarization because the parallel components of current within the helical arms cancel each other, whereas the vertical components are in phase, adding constructively, and contributing to the development of electrical fields. As a result, the antenna resembles a monopole over a ground plane, and has an omni-directional radiation pattern. The radiation pattern is stronger for $\theta \leq 60^o$ as the helical arms are closer at this elevation angle and the currents are more dense, as indicated in Fig. 3, at a top view picture of the simulated antenna. The antenna, as shown in Fig. 1(a) consists of a hemisphere with radius $\rho = 4.8$ mm adjusted on a ground plane with a size of $50\times\times\times37.5$ mm^2. The Rogers 3850 which is copper plated on both sides is used as the ground plane. It has a thickness of 1mil, $\epsilon_r = 2.9$ and $\tan\delta = 0.0025$. The radiating elements of the antenna are the three helical arms mounted on the hemisphere. The wire of the helical arms has a radius of 0.127 mm. Each wire has a length of almost 10 mm. Two of the wires are soldered on the reverse side of the ground plane and one of them is connected to a pigtail, serving as the feed for the antenna. A small hole is opened on the Rogers 3850 so that one of the antenna arms can be connected to a pigtail which is positioned in the other side of the ground. The inner conductor of the pigtail is soldered to the helical arm and the outer conductor is soldered to the copper-plated Rogers 3850 that acts as a ground plane The three arms are connected on the top of the hemisphere through soldering. A reflector is adjusted $\lambda/4$ away from the one side of the antenna, to help boost its performance and protect it from the reflections caused by the metallic body of the vehicle. The antenna was initially simulated using the Ansys Electronics Desktop software. The helical arms were designed following the equation based curve: $x(t) = \sin(t) \times \cos(\frac{t}{2\pi N} - 1) \times \rho$, $y(t) = \sin(t) \times \sin(\frac{t}{2\pi N} - 1) \times \rho$ and $z(t) = \cos(t) \times \rho$, where t is a variable representing the angle swift from 0 to $\frac{\pi}{2}$ as the helical arms are wrapped around a hemisphere. Variable t represents the angular position of the wire radius as also indicated in Fig. 3. N is the number of turns, and for our design is set to N = 1. Finally, $\rho = 4.8$ mm refers to the radius of the hemisphere. The simulated resonance and radiation patterns of the antenna are shown in Figs. 1 and 2. The radiation patterns of E plane are plotted for $\phi = 90°$ and $0^o \leq \theta \leq 180°$. The H-plane patterns are plotted for $\theta = 90°$ and $-180^o \leq \phi \leq 180°$. As indicated in Fig. 1(a), the simulated antenna is placed on the xy plane and the reflector is mounted on the ground plane at $\phi = 270°$.

III. FABRICATION

To fabricate the antenna a $50\times\times\times37.5$ mm^2 copper plated Rogers 3850 is used as a ground plane and a $50\times\times\times25$ mm^2 part of the same material is used as a reflector, similar to the

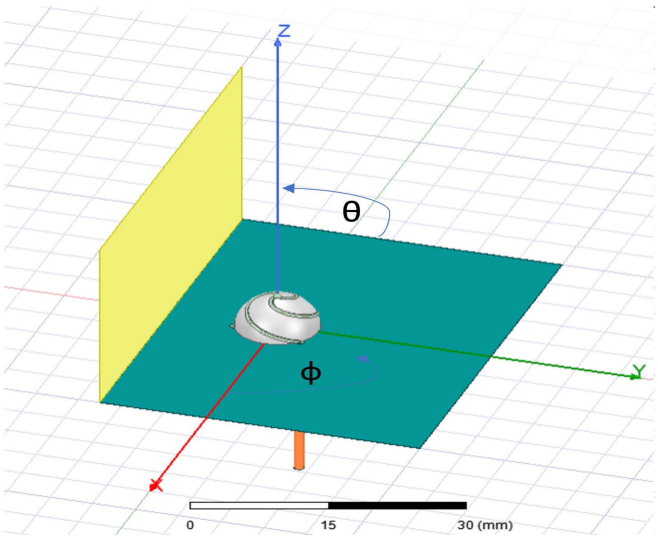

(a)

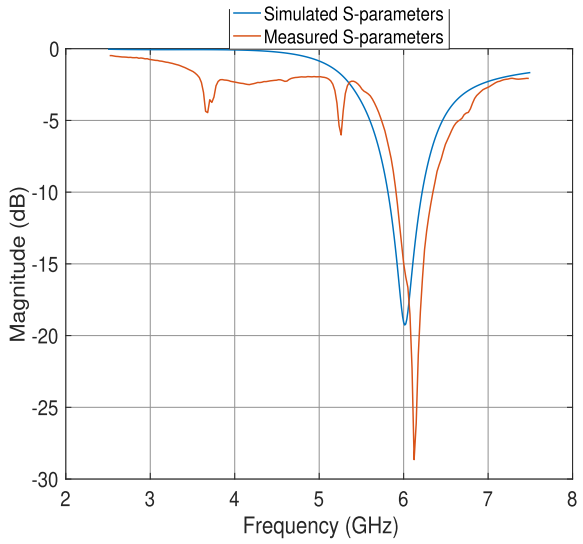

(b)

FIGURE 1. Antenna design as simulated in Ansys HFSS and the simulated versus the measured S-parameters.

simulations. The reflector is placed $\frac{\lambda}{4}$ away from the antenna and it is cut at 25 mm height to be accommodated inside the CHMSL. A hemisphere made by vero-white is 3D printed using the Connex 3D polyjet printer. The vero-white is an opaque polyjet resin that is used to create 3D printed objects. Its base is a photosensitive polymer liquid. It has a permittivity of $\epsilon_r = 2.97$ and $\tan\delta = 0.0285$, as stated in [6], and a heat deflection temperature of 50° C, [7]. The vero-white has a melting temperature similar to many automotive plastics. For the helical radiating elements of the antenna, a 30 AWG wire used. Photos of the fabricated antenna are shown in Fig. 4. The dimension of the ground and reflector were led by the available space (length, width and height) of the CHMSL. The positioning of the reflector is $\frac{\lambda}{4}$ away from radiator. So it is a combination of space availability and electromagnetics. This

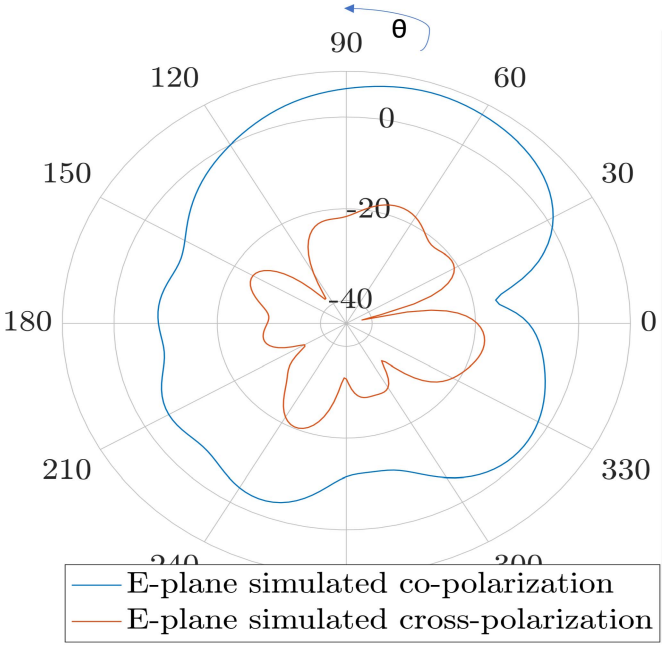

(a)

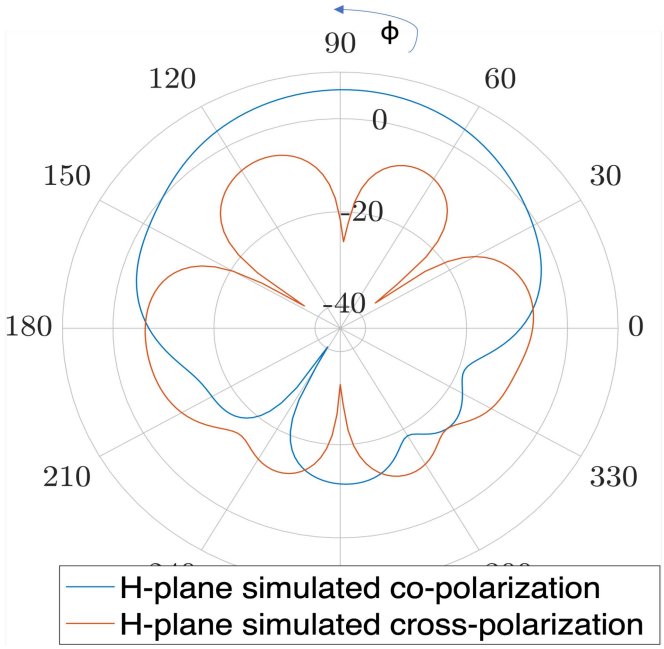

(b)

FIGURE 2. Simulated antenna co- and cross- polarization on E and H planes.

figure shows the ground plane and the reflector before being trimmed to fit in the CHMSL. The ground behind the reflector is removed and the height of the reflector is trimmed at 25 mm to fit in the plastic covering the third stop light.

IV. MEASUREMENTS

After fabricating the antenna, the S-parameters were measured using the M5227 PNA by Keysight Technologies. The

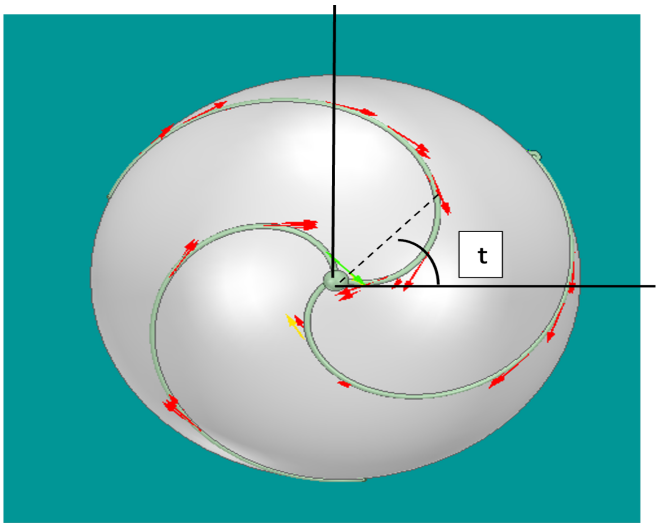

FIGURE 3. Currents on simulated antenna and variable t.

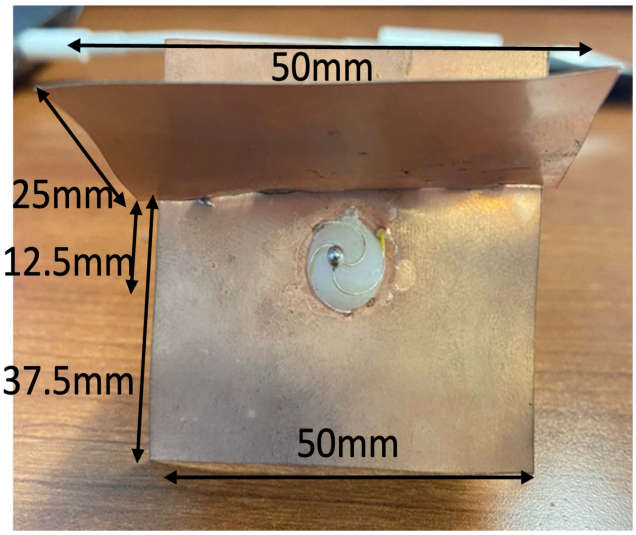

FIGURE 4. Fabricated antenna with pigtail and reflector before trimming reflector and ground to fit in CHMSL.

S-parameters were measured while the antenna was free, not mounted on the vehicle. The antenna was transferred at the Drive-ability Test Facility (DTF) of Ford Motor Company. The MVG3000 M near field system was used to measure the antenna's performance. Three different experiment setups were performed at the DTF; a) the antenna was mounted on a foam pillar and absorbers were adjusted below the pillar to remove any unwanted reflection from the turn table, b) the antenna was mounted on a circular ground plane with a diameter of 1 m and absorbers were adjusted below the ground plane, and c) the antenna was mounted at the rear side of a Ford vehicle around the car high mount stop light (CHMSL) area. We removed the CHMSL from the back of the testing vehicle and opened it so that we can remove the LED. Once the LED is removed the inside of the CHMSL is empty. The LED is

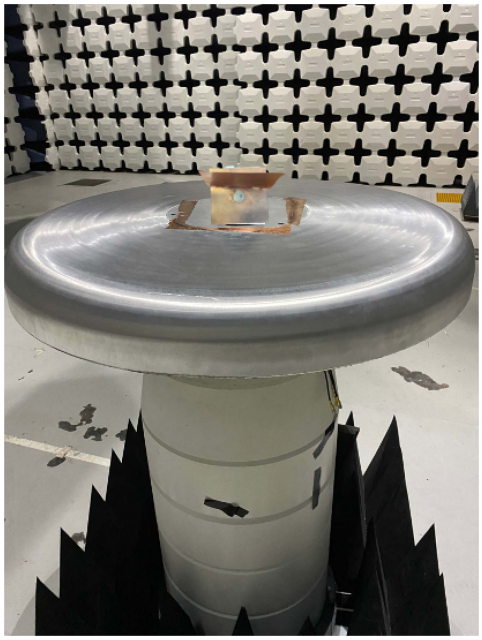

FIGURE 5. Experimental setup B: Ground plane inside MVG 3000 at DTF.

encapsulated inside its own plastic. You can easily remove LED and mount the antenna in the available space behind the LED, as indicated in Fig. 6. Again, absorbers were adjusted around the vehicle and on the walls of the room, as indicated in Fig. 6 to minimize any reflection of the surroundings on the antenna radiation pattern. The two different setups for experiments b) and c) are indicated in Fig. 5 and Fig. 6. The vehicle used during the measurements is a Bronco 2022 with a hard top rooftop, a spare wheel and a CHMSL in the back.

The measured S-parameters of the fabricated antenna - when it is not mounted on a ground plane or on a vehicle- are indicated in Fig. 1(b). The resonance of the fabricated antenna has shifted 100 MHz to higher frequencies. The feeding wire is slightly shorter than the simulated as the pigtail is heavier than the wire of the helical arms, pushing the feeding wire towards the back of the ground and this could justify the 100 MHz higher resonance frequency. However at 5.9 GHz both simulated and fabricated antenna have a return loss better than 10 dB, so the measured and simulated gains are not affected by mismatch losses. Moreover, both simulated and fabricated antennas have a return loss better than 8 dB, between 5850-5925 MHz, as required for C-V2X communications. The measured radiation properties of the antennas when mounted on the ground plane, during experimental setup B, are given in Fig. 7(b). The measured radiation performance of the antenna when mounted in the rear area of the vehicle, during experimental setup C is indicated in Fig. 7(c).

V. RESULTS

All the presented measurement results refer to the C-V2X frequency of 5.9 GHz. The measurement results of the experimental setup A, where the antenna was mounted on the foam

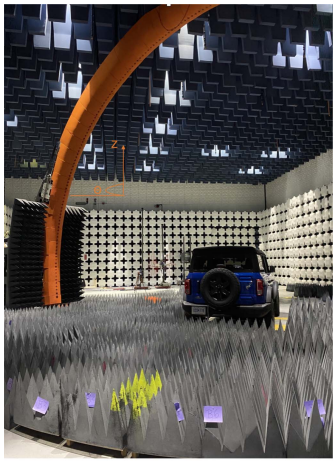

(a)

(b)

FIGURE 6. Experimental setup C: (a) Ford SUV inside MVG 3000 at DTF and (b) antenna inside the CHMSL of the Ford SUV.

TABLE 1. Measurement Results of Antenna on the Foam Pillar (Experiment A) and on the Ground Plane (Experiment B) at DTF

Azimuth Range	Polar Range	Measured Linear Average Realized Gain (dBi)	
		Foam Pillar	Ground Plane
$0^o \leq \phi \leq 60^o$ and $300^o \leq \phi \leq 360^o$	$90^o \leq \theta \leq 96^o$	-6.1	-5.1
	$89^o \leq \theta \leq 91^o$	-3.59	-3.1
	$84^o \leq \theta \leq 90^o$	-2.16	-1.8
	$80^o \leq \theta \leq 84^o$	-1.21	0.3
	$70^o \leq \theta \leq 80^o$	-2.12	1.4
	$50^o \leq \theta \leq 70^o$	-0.77	-1.8

pillar are presented in Table 1 and 2. The measurement results of the experimental setup B where the antenna was mounted on the ground plane are presented in the same Table 1 and 2 and the measurement results of the experimental setup C where the antenna was mounted around the CHMSL area of the Ford vehicle are gathered in Table 3 and 4. The data of the antenna measurements on the pillar of foams and the ground are averaged in Table 1 over the angles $0^o \leq \phi \leq 60^\circ$ and

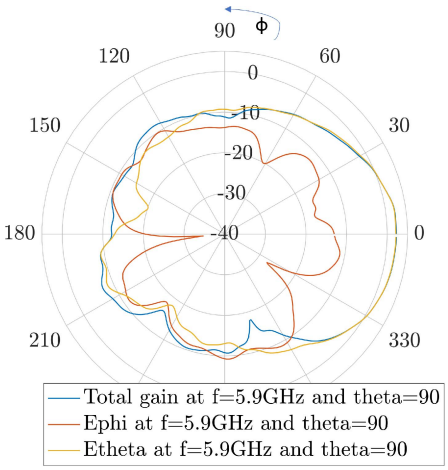

(a)

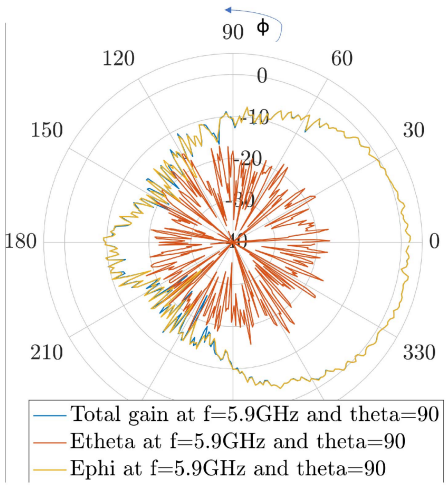

(b)

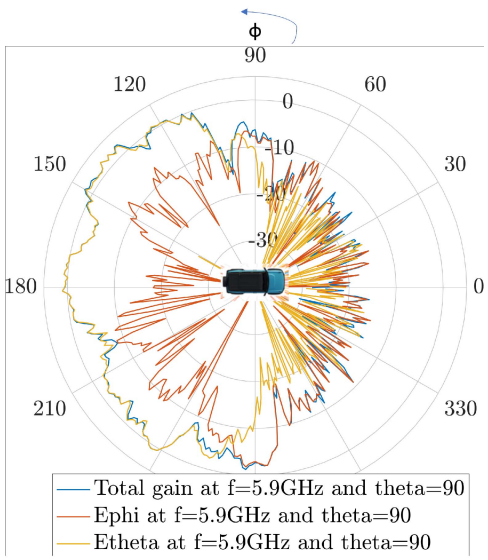

(c)

FIGURE 7. Radiation performance of antenna: (a) when mounted on a pillar of foams; (b) when mounted on the ground plane at DTF; (c) when mounted around the CHMSL of the vehicle inside MVG 3000 at DTF of Ford Motor Company.

TABLE 2. Measurement Results of Antennas on the Foam Pillar (Experiment A) and on the Ground Plane (Experiment B) at DTF

Azimuth Range	Polar Range	Measured Linear Average Realized Gain (dBi)	
		Foam Pillar	Ground Plane
$60^o \leq \phi \leq 90^o$ and $270^o \leq \phi \leq 300^o$	$90^o \leq \theta \leq 96^o$	-12.58	-12.5
	$89^o \leq \theta \leq 91^o$	-3.6	-9.6
	$84^o \leq \theta \leq 90^o$	-14.5	-5.6
	$80^o \leq \theta \leq 84^o$	-13.03	-7.7
	$70^o \leq \theta \leq 80^o$	-9.65	-6.9
	$50^o \leq \theta \leq 70^o$	-9.07	-11.2

TABLE 3. Measurement Results of Antenna Inside the CHMSL of Ford Vehicle at DTF (Experiment C)

Azimuth Range	Polar Range	Measured Linear Average Realized Gain (dBi)
$120^o \leq \phi \leq 240^o$	$90^o \leq \theta \leq 96^o$	-3.8
	$89^o \leq \theta \leq 91^o$	-3.5
	$84^o \leq \theta \leq 90^o$	-2.8
	$80^o \leq \theta \leq 84^o$	-2.4
	$70^o \leq \theta \leq 80^o$	-2.9
	$50^o \leq \theta \leq 70^o$	-4.4

TABLE 4. Measurement Results of Antenna Inside the CHMSL of Ford Vehicle At DTF (Experiment C)

Azimuth Range	Polar Range	Measured Linear Average Realized Gain (dBi)
$90^o \leq \phi \leq 120^o$ and $240^o \leq \phi \leq 270^o$	$90^o \leq \theta \leq 96^o$	-7
	$89^o \leq \theta \leq 91^o$	-6.5
	$84^o \leq \theta \leq 90^o$	-5.9
	$80^o \leq \theta \leq 84^o$	-4.9
	$70^o \leq \theta \leq 80^o$	-5.9
	$50^o \leq \theta \leq 70^o$	-8.8

$300^o \leq \phi \leq 360°$ on the azimuth range. The dB values retrieved by the MVG chamber are averaged over the mentioned angles. The antenna has a reflector at $\phi = 180°$ and is centered under the sensor of the MVG 3000. As a result, the maximum gain of the antenna is expected at $\phi = 0°$. In Table 2 the gain of the antenna is averaged over the azimuth range of $60^o \leq \phi \leq 90°$ and $270^o \leq \phi \leq 300°$. Again, the reason for averaging over this range is that the antenna is centered under the top sensor of the MVG 3000 system and the expected maximum value of realized gain is at $\phi = 0°$, but we are

TABLE 5. Maximum Measured Realized Gain of Antennas at the Three Different Experimental Setups

Experimental Setup	Max Measured Linear Average Gain (dBi)	Elevation Angle θ
A - antenna on the foam pillar	-0.77	$50^o \leq \theta \leq 70^o$
B - antenna on the ground plane	1.4	$70^o \leq \theta \leq 80^o$
C - antenna mounted on the rear area of vehicle	-2.4	$80^o \leq \theta \leq 84^o$

TABLE 6. Comparison of Antenna Performance in C-V2X

Paper	Antenna Size (mm^3)	Simulated Max Gain (dBi)
[9]	$50 \times 17 \times 1.1$	2.13
[2]	$\pi \times 25^2 \times 4$	4.5
helical antenna	$50 \times 37.5 \times 25$	3

interested to evaluate the degradation of the antenna radiation at the sides of the SUV.

During the experiment C, when the antenna is placed in the rear area of the vehicle, the top sensor of the MVG 3000 system is centered over the top of the antenna, and the front of the vehicle is at $\phi = 0°$, so the maximum of the antenna is expected at $\phi = 180°$. This is the reason the gain of the antenna is averaged over $120^o \leq \phi \leq 240°$, $90^o \leq \phi \leq 120°$ and $240^o \leq \phi \leq 270°$ in Tables 3 and 4. Since the antenna is placed in the center back of the vehicle, where $\phi = 180°$, it makes sense to test the antenna radiation performance in the azimuth range of $90^o \leq \phi \leq 270°$. In Table 5, we have gathered the maximum measured realized gain values of the antenna at the three different experimental setups and the elevation angle where the maximum was measured.

The elevation angles of interest are the $89^o \leq \theta \leq 91°$ which refer to the performance of the antenna at the horizon. For the azimuth angles $0^o \leq \phi \leq 60°$, $300^o \leq \phi \leq 360°$ and $120^o \leq \phi \leq 240°$, where we average over the part of the antenna that is in front of the reflector, we observe that the measured realized gain is 0.5-1 dB better when the antenna is placed on the infinite ground plane, compared to the foam pillar, for the elevation angles of $70^o \leq \theta \leq 96°$. When the antenna is mounted on the rear area of the vehicle, the linear average realized gain is 1.3 dB better compared to the values of the linear average realized gain of the antenna on the ground plane for $90^o \leq \theta \leq 96°$. For the rest of the elevation angles, the performance of the antenna when mounted around the CHMSL area, is almost 1 dB worse than the ground plane placement. For $\theta \leq 90°$ the antenna performance is affected by reflections created by the vehicle metallic body, which is behind the antenna and above the reflector. At the antenna mounting position, for $\theta \geq 90$ there is a spare wheel below the antenna which protects it from the metallic body of the vehicle. From Table 5, where the maximum measured linear average realized gain of the antenna at the different experimental setups is gathered, we can see that the fabricated antenna has maximum values for $0^o \leq \theta \leq 84°$. This is expected as the design of the antenna results in more dense fields at the top of the hemisphere, $\theta \leq 84$. The helical arms are closer to each other and there are more currents at that point. However, for each setup the maximum value is observed at different θ range but always for $\theta < 90$. When the antenna is placed on the foam pillar, the maximum gain is measured for $\theta \leq 74°$ which is expected as there are no reflections from the vehicle body as in the third setup, where the antenna is mounted at the CHMSL area of the vehicle. The existence of metal parts around the antenna creates reflections which affect the antenna performance and move the maximum gain to θ values closer to 90°. When comparing the radiation performance of the antenna on the pillar of foams and the ground, as indicated in Fig. 7, the antenna's cross-polarization level is lower during the experimental setup B, where the antenna was mounted on the infinite ground plane. Moreover the maximum realized gain increases when there is an infinite ground plane. However, the radiation patterns of the antenna are not as smooth as when they are measured on the foam pillar. During the experimental setup C where the antenna is measured around the CHMSL area of the vehicle, the cross-polarization level increases and the radiation pattern of the antenna develops some lobes. At this position the antenna has no infinite ground plane and there are reflections created by the vehicle body, the spare tire adjusted below the mounting position of the antenna and other vehicular metal parts above and behind the antenna.

The requirements for antenna performance at C-V2X are specified by each automotive company, following the SAE J3161 standards [8] that are developed based on 3GPP and ETSI requirements. According to ETSI Release 14, the on board unit for C-V2X applications should have a Packet Error Rate (PER) less than 10% which occurs for a range of 300 m. Moreover the maximum transmitted power is 23 dBm. We gathered some information regarding published C-V2X antenna performance in Table 6, to gain a better understanding about C-V2X antenna performance requirements. By comparing the simulated maximum realized gain of the antenna proposed to this article to the simulated maximum realized gain of C-V2X antenna developed in [9], it is found that the simulated gain of our antenna is 1 dB better compared to the [9] and 1.5 dB worse compared to [2]. This is expected as the size of the antenna presented in [2] is the largest compared to the other two. Both antennas for C-V2X communications, found in literature have a simulated return loss better than 8db at 5850–5925 MHz, omni-directional radiation pattern and vertical polarization which are requirements for C-V2X communications.

VI. CONCLUSION

A helical antenna was implemented on the 3D printed vero white material. The suggested antenna was tested under three different experimental setups; a)mounted on a foam pillar, b)on an infinite ground plane and c)in the rear CHMSL of a real vehicle for the first time to the best of our knowldege, resulting in adequate performance for C-V2X communications.

This research introduces for the first time, the CHMSL area of an SUV vehicle as a successful candidate placement of automotive antennas. By measuring the antenna on an infinite ground plane that resembles the rooftop of a vehicle and comparing its performance at the new mounting position (CHMSL area) to the infinite ground plane and free space measurements, we verified that the CHMSL area allows normal operation of the C-V2X antenna and can mitigate the number of automotive antennas mounted on the rooftop. Moreover, it is the first time that a helical has been tested for C-V2X communications and its performance meets the requirements for successful transmission. The size of this antenna allows its mounting around the CHMSL area, without impeding the driver or the aesthetics of the vehicle, while presenting adequate performance. However, a second similar antenna should be placed at the front of the vehicle to cover the 360°.

The presented antenna can be additively manufactured and further reduce the cost of its development, making it a candidate for mass production in automotive industry.

REFERENCES

[1] A. Jouini, S. Hasnaoui, and A. Cherif, "Comparative study of patch antennas for C-V2X communication," in *Proc. IEEE 5th Int. Conf. Adv. Syst. Emergent Technol.*, 2022, pp. 61–66.

[2] Y. Zhou, G. Zhao, Y. J. Zhang, and M. S. Tong, "An omnidirectional vertical-polarized C-V2X antenna with high gain and low profile," in *Proc. IEEE Int. Symp. Antennas Propag. USNC-URSI Radio Sci. Meeting*, 2021, pp. 1956–1957.

[3] R. R. Alavi, A. Harb, and D. N. Aloi, "Comparison of NF and FF automotive antenna measurement in DSRC and C-V2X applications," in *Proc. IEEE Int. Symp. Antennas Propag. USNC-URSI Radio Sci. Meeting*, 2022, pp. 780–781.

[4] H. Shen and C.-C. Chen, "A flush mount automobile 4-channel universal antenna design," in *Proc. IEEE Int. Symp. Antennas Propag. USNC-URSI Radio Sci. Meeting*, 2022, pp. 475–476.

[5] S. R. Best, "The radiation properties of electrically small folded spherical helix antennas," *IEEE Trans. Antennas Propag.*, vol. 52, no. 4, pp. 953–960, Apr. 2004.

[6] R. L. Dumene, P. Kennedy, C. B. Williams, D. Sweeney, and G. Earle, "Creating embedded radiofrequency structures using polyjet material jetting," in *Proc. Int. Solid Freeform Fabr. Symp.*, 2015, pp. 1769–1787.

[7] Inc Stratasys, "Vero material properties," 2008. Accessed: 2023. [Online]. Available: https://www.stratasys.com/siteassets/materials/materials-catalog/polyjet-materials/verovivid/mds_pj_vero_for_j55_0320a.pdf

[8] SAE, "On board system requirements for lte v2x - v2v safety communications," 2022. Accessed: 2023. [Online]. Available: https://www.sae.org/standards/content/j3161/1_202203/preview/

[9] R. Vasudevan and V. Nagaraju, "Miniaturized semi-hexagonal aperture shape antenna with elliptical ground for C-V2X communication," in *Proc. Int. Conf. Automat., Comput. Renewable Syst.*, 2022, pp. 233–238.